*Geophys. J. Int.* (2003) **155,** 1–10

# *P* wave amplitudes in a 3-D earth

Ileana M. Tibuleac,[1,*] Guust Nolet,[1] Caryl Michaelson[1] and Ivan Koulakov[2]

[1] *Geosciences Department, Princeton University, Princeton, NJ* 08540
[2] *GeoForschungsZentrum Potsdam, Potsdam, Germany*

Accepted 2003 February 15. Received 2002 December 28; in original form 2002 April 22

## SUMMARY

Evidence is presented here that *P* wave amplitudes contain additional information on the Earth's heterogeneity and must be considered in future tomographic interpretations. We analyse the reliability and the variance of teleseismic *P* wave amplitudes recorded at well calibrated broadband Global Seismic Network (GSN) stations from intermediate to deep earthquakes (depth >46 km). The dataset contains 217 earthquakes with $m_b$ between 5.6 and 7.6, from 1993 January to 2000 May. Using pairs of closely located events with similar focal mechanisms as well as data recorded at the closely spaced MOMA seismic array we demonstrate the consistency of observations. We deduce that the magnification of the GSN instruments generally drifts by at most 2 per cent per year, and likely much less. *P* wave amplitudes have variations due to focusing/defocusing with a standard deviation of at least 38 per cent. This reduces to 19 per cent if only periods in excess of 10 s are considered. Tomographic *P* wave models with mantle velocity anomalies of the order of 1 per cent are unable to reproduce such large variations.

**Key words:** instrumentation, mantle heterogeneity, *P*-wave amplitudes.

## 1 INTRODUCTION

Tomographic models of *P*-wave velocity in the Earth are so far only based on traveltime anomalies. The goal of this study is to assess if variations in *P*-wave amplitudes can add to that information, despite difficulties involved in both observation and interpretation. Here we report results obtained for *P*-wave amplitudes observed from intermediate and deep earthquakes for which the measurement and interpretation are less complicated.

Amplitudes of seismic waves are used to assess the seismic event magnitudes, and there has been a continuous effort to understand amplitude variations on local, regional and global levels. Studies of variations of the short period *P*-wave amplitudes across large seismic arrays such as LASA and NORSAR have shown that the amplitude of a given signal can differ by a factor of four or more between seismometers separated by only a few kilometres (Douglas *et al.* 1981). Short period amplitudes of explosions closely located and of close yield can vary as much as 90 per cent (Romney 1959). Short period amplitudes are strongly influenced by the lithology beneath the receiver (Lay & Helmberger 1981; Marshall *et al.* 1986). They also depend on variations of attenuation in the upper mantle (Booth *et al.* 1974; Lay & Helmberger 1981) or may be due to shallow lens-like structures (Haddon & Husebye 1978). Despite the difficulty in predicting amplitude fluctuations at individual sites, regional averages of magnitude residuals for short period waves were found to be still meaningful (Der *et al.* 1982). Variations of long period *P* waves are less dramatic, and correlations with the geological character of the lithosphere or crust have been noted (Douglas *et al.* 1981; Der *et al.* 1982; Booth *et al.* 1974; Lay & Helmberger 1981).

Amplitudes have not yet been exploited in a systematic way to provide a check on accuracy of tomographic models. It seems also timely to investigate the reliability of amplitudes observed with newer, high quality digital instrumentation. In this study we present long period (>4.5 s) *P*-wave amplitude measurements at the GSN stations from intermediate to deep earthquakes and compare our measurements with theoretical predictions, both for the radial model IASPEI91 (Kennett 1991) and for two representative 3-D models.

## 2 DATA

We analysed *P* waveforms from 217 earthquakes (Fig. 1) at depths between 46 and 565 km, with $m_b$ magnitudes between 5.6 and 7.6. The events were recorded between 1993 January and 2001 May at well calibrated broadband global stations as well as at some temporary networks. *P*-wave arrivals were semi-automatically picked on the vertical component of stations 35°–88° from the epicentre, so as to avoid influence from upper-mantle discontinuities or D″. We selected only data with a good signal-to-noise ratio and P well separated from pP or PcP arrivals. When we observed complex waveforms, we accepted only seismograms with similarly shaped initial pulses. This resulted in a total of 5234 amplitude measurements, that were subsequently culled down by rejecting 39 per cent of the observations using additional selection criteria (as discussed below).

*Now at: Weston Geophysical Corporation, 57 Bedford St., Suite 102, Lexington MA 02420.

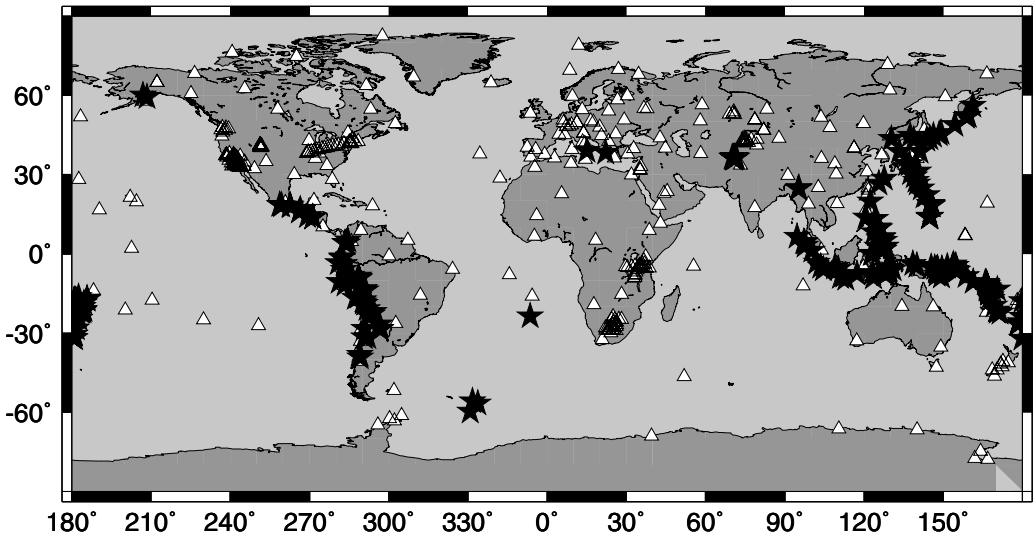


**Figure 1.** GSN stations used in this study (triangles) and the earthquake epicentres (stars).

## 3 METHOD

We define the teleseismic *P*-wave amplitude as the square root of the energy, i.e. the rms amplitude:

$$A = E^{\frac{1}{2}} = \left[\int s(t)^2\, dt\right]^{\frac{1}{2}} \tag{1}$$

where $s(t)$ are displacement pulses low pass filtered at 0.2 Hz. Long period trends in the baseline were subtracted from $s(t)$. We found this rms amplitude to be a relatively stable measurement compared to zero-to-peak or peak-to-peak amplitude. Typical data quality is shown in Fig. 2, which shows the filtered waveforms from a Fiji Islands Region event on 1999 April 13, $m_b = 6.8$ at 164 km depth.

To first order of accuracy, we assume that the theoretical expression for the body wave energy can be expressed as

$$E = f_s^2 f_r^2 \mathcal{R}^{-2} a_s a_r \tag{2}$$

or

$$\log E = \log f_s^2 + \log f_r^2 + \log \mathcal{R}^{-2} + \log a_s + \log a_r \tag{3}$$

where $-1 \leq f_s \leq 1$ is a source radiation factor calculated from the Harvard CMT solution, $f_r$ is the free surface effect at the receiver (Dahlen & Tromp 1998), $\mathcal{R}$ is the geometrical spreading coefficient calculated for a particular 3-D model and $a_s$ and $a_r$ are the source and receiver corrections respectively.

The largest unknowns in eq. (3) are $\mathcal{R}$, $a_s$ and $a_r$. We may estimate $f_r$, $f_s$, and $\mathcal{R}$ from source and velocity models. Since estimates of scalar moment for the same event often differ by factors that are comparable to the variations in amplitude we observed, $a_s$ cannot be calculated reliably *a priori* from published scalar moments and regional attenuation models. Similarly, present knowledge of receiver structure under the GSN stations is inadequate for removing receiver effects *a priori*.

We use eq. (3) to solve for $\log a_s$ and $\log a_r$ by regression on the full collection of measurements assuming $\mathcal{R}$ for a particular model to be correct. This way, the corrections are used to optimize agreement between the data and the model, and any remaining discrepancies are therefore a conservative measure of the inadequacy of the model—most likely due to the highly uncertain estimate of $\mathcal{R}$.

This regression problem is underdetermined by a constant factor. For example, halving all stations corrections while at the same time doubling the receiver corrections would not affect the fit to eq. (3). Therefore no physical significance should be assigned to these factors. To resolve the ambiguity, we forced the geometrical average of all station corrections to be unity: $\Pi_i a_{si} = 1$.

The corrections $a_s$ and $a_r$ serve to absorb local effects common to all events and all stations (including the attenuation in the local asthenosphere), considering that the effects of variation of attenuation in the deep mantle are negligible (Booth *et al.* 1974; Choy & Cormier 1986). The receiver correction term $a_r$ may absorb effects of focusing/defocusing directly beneath the station, which ideally should be part of the geometrical spreading factor as predicted by a 3-D model. For short wavelength variations in the Moho, the effect is negligible, since amplitude effects on short period waves are healed before they reach the surface. We verified this by using a simple analytical model for wave front healing such as in Nolet & Dahlen (2000). Long wavelength variations have a very small effect on amplitude only a short distance away from the Moho. So the largest effect is for Moho variations at intermediate scale (100–200 km). These are too short to be included in present day 3-D models and in our case are absorbed within the receiver correction. Thus, remaining discrepancies are a conservative estimate of the inadequacy of the model used to predict the geometrical spreading. If $\mathcal{R}$ is computed from a 1-D model, the misfit to eq. (3) indicates the degree of focusing/defocusing imposed by the 3-D Earth.

Events with less than 6 station recordings were rejected and we took care that errors in $f_s$ and $f_r$ would not severely affect the solution of eq. (3). To minimize errors in the radiation factor we discarded the stations for which the radiation factor was less than 0.4. We rejected Harvard CMT solutions that had a poor fit to the observed polarities. An example of observed *P*-wave amplitudes with their sign is given in Fig. 3 for the same event as in Fig. 2. The Harvard CMT solution is shown as a beach ball and the radiated amplitude is projected in gray scale onto the Earth's surface. Despite a strong correlation in trend between predicted and observed *P*-wave amplitudes, amplitude variations from the predicted values still exist, to the order of several tens of per cent. Errors of several percent in $f_s$ are possible if the fault plane orientation is wrong by several degrees. In the future, when more data becomes available to

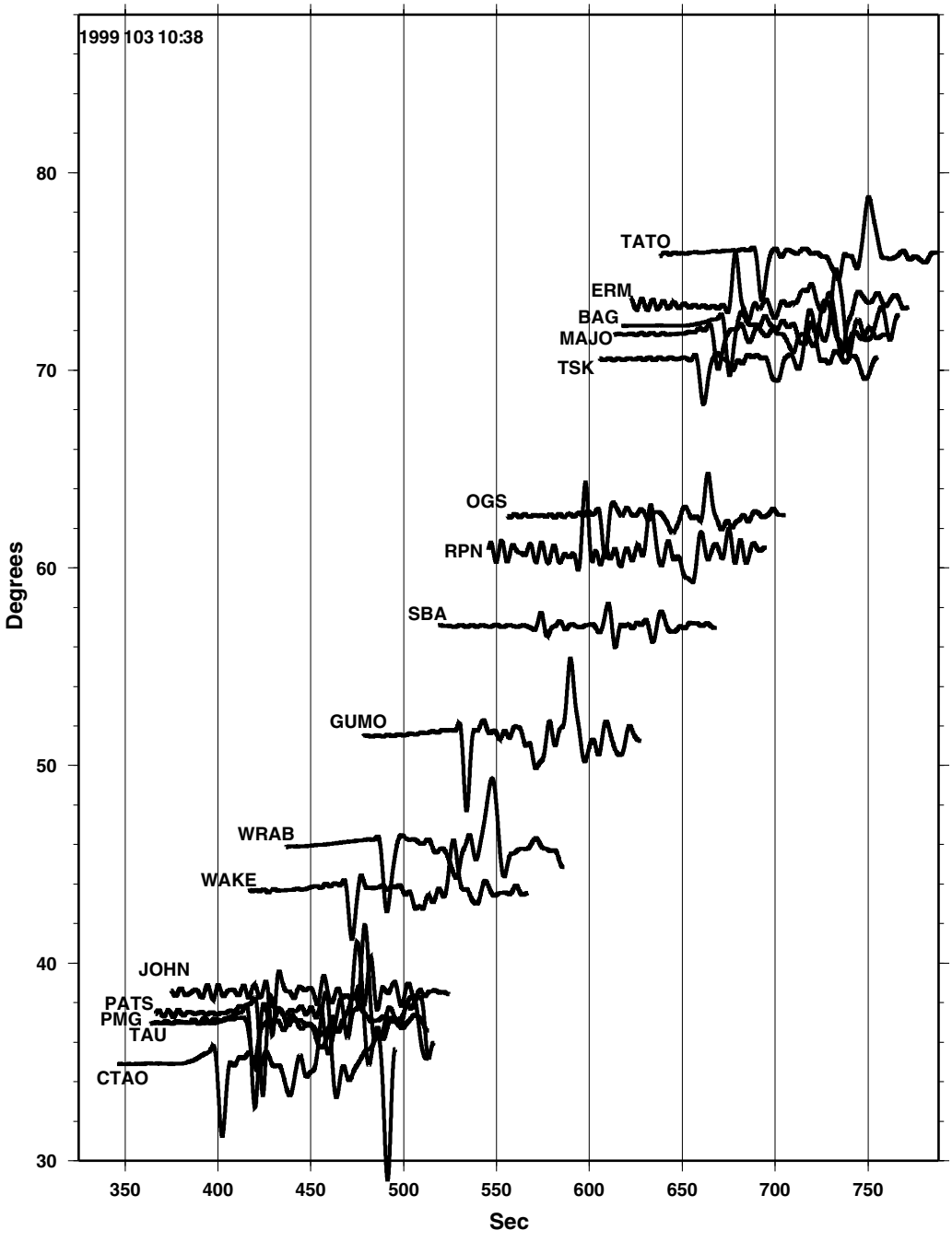


**Figure 2.** Typical recorded waveforms aligned by epicentral distance from a Fiji Islands Region event on 1999 April 13, mb = 6.8, 164 km depth.

make this possible, the moment tensor itself should be incorporated in the regression scheme (3). Estimates of the errors in $f_r$ are less than 5 per cent. The errors are due to possible variation in *P* to *S* velocity ratios beneath the receiver. By selecting only *P* pulses longer than 4.5 s we may assume that $a_s$ is frequency independent (Zhou *et al.* 2002).

## 4 GEOMETRICAL SPREADING

We calculated $\mathcal{R}$ for each event at a certain station by ray tracing through several earth models. None of the currently available tomographic models incorporates amplitude information. In fact, the 1999 version of 3DglobalP (Van der Hilst *et al.* 1997) and SB10L18 (Masters *et al.* 1999) are parametrized in blocks which makes them clearly unfit for adequate prediction of focusing effects. To investigate whether current 3-D tomographic models exhibit focusing that is qualitatively comparable to what is observed, we construct two models:

(1) Model A is constructed by smoothing the 10 × 10° model SB10L18 over caps of 5° radius horizontally.

(2) Model B is derived from the 2 × 2 degree model 3DglobalP by tri-linear interpolation.

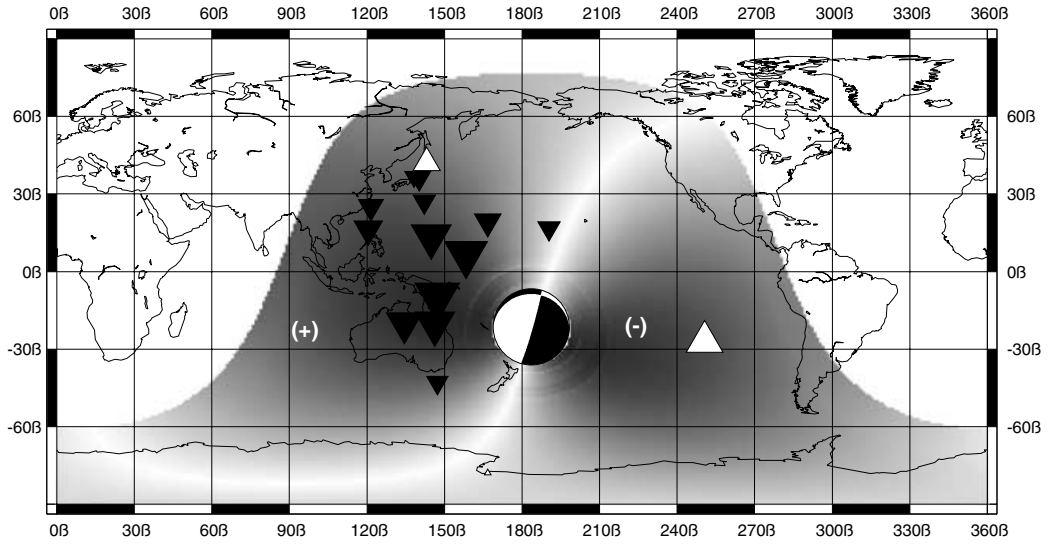


**Figure 3.** The radiated amplitude factor as predicted by the Harvard CMT solution for the Fiji Islands Region event on 1999 April 13, mb = 6.8, 164 km depth, projected in greyscale onto the Earth's surface (the − sign denotes dilation, + represents compression). White triangles represent dilatational arrivals, black triangles represent compressional arrivals, with the size of the symbol proportional to the *P* wave amplitude. One station polarity (ERM, Japan) is reversed. Such obvious reversals have been corrected in the analysis. Plots like this are used to check the quality of the moment tensor solution.

Both models are incorporated in a Cartesian grid with a node spacing of 129 km for model A and 103 km for Model B and added to IASPEI91 (Kennett 1991) to produce absolute velocities by trilinear interpolation. The geometrical spreading for the 3-D models was calculated by finite differencing of rays leaving the source at 1° intervals (Cerveny *et al.* 1977), an intensive computational enterprise typically taking two hours per event on a Pentium III workstation. Fig. 4 presents the amplitude variations due to geometrical spreading for the Fiji Islands Region event from Fig. 2 obtained by 3-D ray tracing for Model A (top) and Model B (bottom). At the bottom we present the amplitude variation relative to the IASPEI91 model (Ao). The concentric anomalies visible in Fig. 4 can be understood because model A is much smoother in the horizontal direction, where it was based on 10 × 10° averages, than in the vertical direction. The tectonic setting for this event (Tonga – Fiji) is complicated. Amplitude anomalies varying between −20 per cent and +30 per cent located near 50 degrees distance in the NNW direction are probably caused by strong focusing/defocusing due to low velocities bordering the high-velocity slab. The focusing in the ESE direction is less easily explained. Note that these anomalies are absent in model B (Fig. 4, bottom), which has more detailed structure in the horizontal direction. In fact, it is difficult to see much agreement between the two models. Large anomalies such as shown in Fig. 4 are not abundant. In fact, the great majority of geometrical spreading values predicted by the 3-D global models deviate by less than about 10 per cent from the IASPEI91 predictions. In more than a million and a half rays we traced, only about 6 per cent of the amplitudes are over 15 per cent and 1 per cent are over 30 per cent different from IASPEI91.

In summary, the steps we took were as follows:

(1) measure the rms amplitude;
(2) predict $f_s$, $f_r$, $\mathcal{R}$ from source/velocity models;
(3) determine $a_s$ and $a_r$ by regression from eq. (3);
(4) use these $a_s$ and $a_r$ to predict the theoretical amplitude;
(5) compare observed and theoretical amplitude values.

## 5 CONSISTENCY OF AMPLITUDE OBSERVATIONS

Because of the absence or lack of reliability of the calibration of older instruments, as well as the absence of reliable moment tensors until the late 1970's, amplitudes have not been incorporated in global seismology studies. Our data set provides a unique opportunity to investigate whether the new generation of broadband, digital instruments yields more consistent amplitude observations.

We investigated the consistency of amplitude observations by inspecting measured amplitudes for cases where we expect the amplitudes to be very similar. For this, we used two approaches:

(1) a study of selected event pairs (Table 1) with close epicentres (less than 1° separation) and very similar moment tensors, and
(2) a study of waveforms recorded at the MOMA array (Fisher *et al.* 1996) to inspect consistency along the array for events from similar azimuths.

Event pairs with similar source mechanism are rare in our data set. In Table 1 we present the six locations of such events for which we had at least six stations with amplitude observations for both events,

**Table 1.** Event pairs.

| Pair | Date | Long | Lat | Depth (km) |
|---|---|---|---|---|
| 1 | 1995/05/16 | 70.9° | 36.3° | 189 |
| | 1995/10/18 | 70.4 | 36.3 | 226 |
| 2 | 1999/01/28 | 153.7 | −4.6 | 101 |
| | 1995/08/19 | 153.9 | −4.9 | 73 |
| 3 | 1998/05/27 | 159.5 | 52.1 | 48 |
| | 1994/02/14 | 158.9 | 51.7 | 43 |
| 4 | 1998/11/14 | 167.5 | −14.8 | 122 |
| | 1996/03/17 | 167.5 | −14.7 | 160 |
| 5 | 1995/08/17 | 170.5 | −21.7 | 90 |
| | 1995/10/09 | 170.2 | −21.3 | 110 |
| 6 | 1998/12/27 | −176.4 | −21.6 | 144 |
| | 1999/04/13 | −176.4 | −21.4 | 164 |

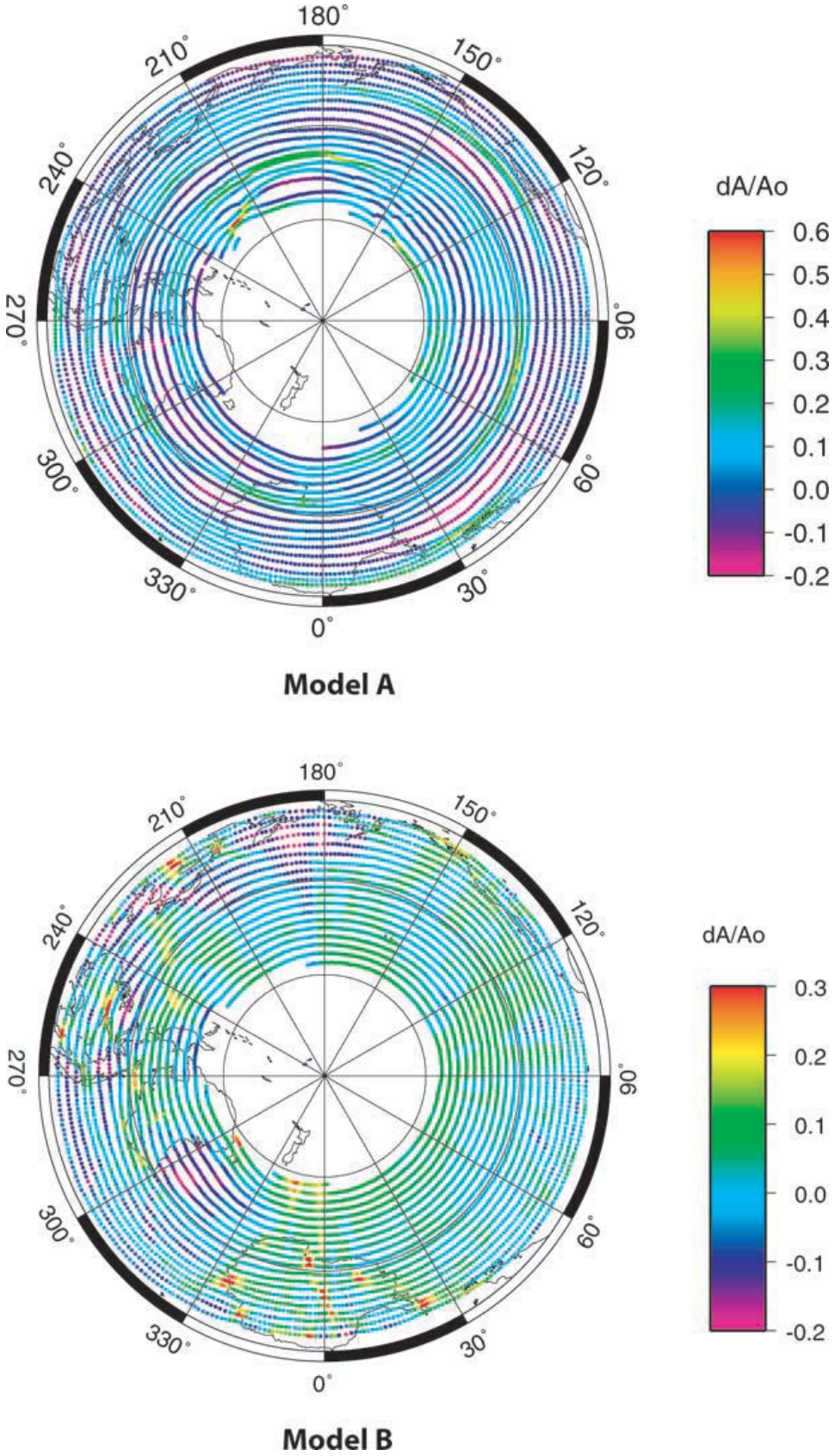


**Figure 4.** Top: The value of geometrical spreading relative to the IASPEI model (Ao) for the Fiji Islands Region, 1999 April 13, mb = 6.8, 164 km depth event, obtained from 3-D ray tracing through Model A. Bottom: the same event, but now with the geometrical spreading computed for model B.

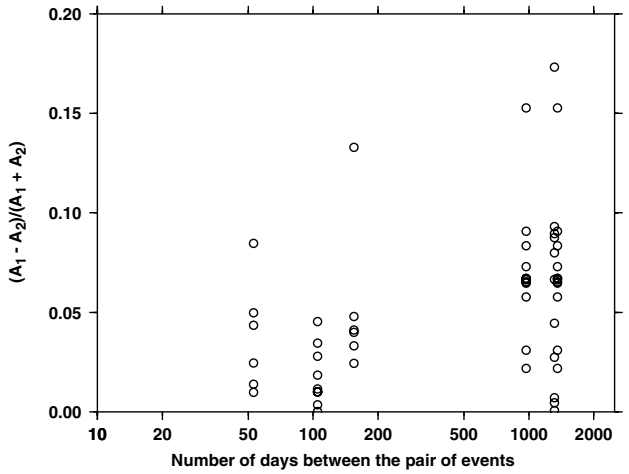


**Figure 5.** Relative amplitude differences $|A_1 - A_2|/(A_1 + A_2)$ as a function of the time span between the pair of events.

allowing for an accurate scaling between the two scalar moments. We also correct for the radiation pattern from the source as the two source mechanisms are similar but not exactly the same. Any remaining differences should be due to strong fluctuations in the source radiation factor, or to focusing effects that are critical to the source location. We note that Pankow & Lay (2002) observed rather strong amplitude effects depending on the location of the source within a subducting slab. The station correction factors should be exactly the same unless the error in the station magnification has changed over time. We verified that the scatter in amplitude observations between the two stations was not decreasing as a function of increasing $f_s$ – an indication that errors in the source mechanism, which would dominate near the nodal lines, are not a major source of error.

Fig. 5 shows the relative amplitude difference $|A_1 - A_2|/(A_1 + A_2)$ with $A_1$ and $A_2$ the two amplitude measurements, as a function of the time span between the pair of events. Most observation pairs are within 5 per cent of the average amplitude if the events are separated by less than a year. But for the two events separated by 1000 days or more, we see a significant increase in the relative difference. This indicates that a 5 per cent error in the instrument magnification (Davis, personal communication, 2001) is probably realistic. It is not unreasonable to assume that the increase from errors of a few per cent at short term, to 7 or 8 per cent for longer time separations is due to instrument drift. Taking into account an extra factor of $\sqrt{2}$ (as our difference subtracts two errors), we conclude that a data set with amplitudes observed over a time span of several years probably has errors due to instrument miscalibration less than 6–7 per cent or limiting the drift to less than about 2 per cent per year. This is a pessimistic estimate, assuming the rays are close enough in each pair that focusing effects are exactly the same. Small scale structure can easily contribute to the difference (Pankow & Lay 2002), but not to the time dependence, indicating that the instrument effects are at least 1–2 per cent over the full time span of three years in Fig. 5. Note that this is still much smaller than the observed range of amplitude variations that we shall present later. The outliers in Fig. 5 belong to a few stations that have apparently drifted more than others: LBTB (Lobatse, Botswana, Africa), PSI (Propat, Indonesia) and CTAO (Charters Towers, Australia).

We now turn to our second test, and will inspect measured $P$ energy for the closely spaced MOMA stations (Table 2). $P$ wave

**Table 2.** MOMA array stations.

| Station | Lat | Long |
|---|---|---|
| MM01 | 42.3° | −72.7° |
| MM02 | 42.2 | −73.7 |
| MM03 | 42.0 | −74.8 |
| MM04 | 41.8 | −76.2 |
| MM05 | 41.6 | −76.9 |
| MM06 | 41.4 | −78.1 |
| MM07 | 41.2 | −79.1 |
| MM08 | 41.1 | −80.1 |
| MM09 | 40.8 | −81.2 |
| MM10 | 40.6 | −82.3 |
| MM11 | 40.2 | −83.2 |
| MM12 | 40.0 | −84.4 |
| MM13 | 39.8 | −85.3 |
| MM14 | 39.5 | −86.4 |
| MM15 | 39.3 | −87.3 |
| MM16 | 38.9 | −88.3 |
| MM17 | 38.7 | −89.3 |
| MM18 | 38.5 | −90.6 |

**Table 3.** Location of events recorded at MOMA array.

| Date | mb | Lat | Long | Dist | Azim | Depth (km) |
|---|---|---|---|---|---|---|
| 1995/02/08 18:40 | 6.4 | 4.0° | −75.6° | 37° | 172° | 71 |
| 1995/05/02 06:06 | 6.7 | −3.8 | −76.9 | 46 | 172 | 97 |
| 1995/08/03 08:18 | 5.8 | −28.1 | −69.2 | 70 | 168 | 100 |
| 1995/08/19 21:43 | 6.6 | 5.1 | −75.6 | 37 | 167 | 120 |
| 1995/09/23 22:31 | 6.4 | −10.7 | −78.5 | 51 | 172 | 67 |

amplitudes from five 1995 earthquakes (Table 3) are represented at each station in Fig. 6 as triangles. The source radiation factor $f_s$ (continuous line) varies smoothly between the stations. There is an obvious difference in amplitudes for the same earthquake between the eastern and western stations (Figs 6a–c, e) for closer (37 to 46° epicentral distance as well as for farther (70° epicentral distance) events. Fig. 6(d) is an exception: the amplitudes of the event 1995/09/23 22:31, located at 50° epicentral distance vary smoothly across the array. Unfortunately in this case the easternmost stations are not represented in the data set. The MOMA amplitudes are dominated by the low wavelength patterns of amplitude variations. Small excursions from this pattern are not generally consistent between events, and allow us to give an upper estimate of the observational error, which is of the order of 5 per cent, consistent with the conclusion we reached from the analysis of event pairs. If the variations in amplitude (as large as 40 per cent, see subplot Fig. 6c) were due entirely to the near receiver effect, we would observe a consistent pattern at the array as all our events come from the same back azimuth. MM06 has larger amplitudes than the other stations and the crust is thicker beneath the eastern stations 1 to 8 (the western Appalachian orogen) but we think this is not the cause of the amplitude variations we observe. The high amplitude in MM06 is part of a pattern, visible in subplots a to c and e, where there is a clear increase in amplitude as we go from station 10 and 8. However, the magnitude of this increase differs with event location and is absent for the event in subplot d. The source radiation factor varies smoothly therefore the effect is not due to variations in source radiation pattern. Aside from focusing, a possible explanation for the effect is the existence of 3-D heterogeneity in attenuation in the upper mantle. We consider it is not strong enough to cause variations in excess of 40 per cent as we observe. For example a 6 s $P$ wave traversing a 100 km layer of $Q_P = 300$ would attenuate by 4 per cent, twice that caused by

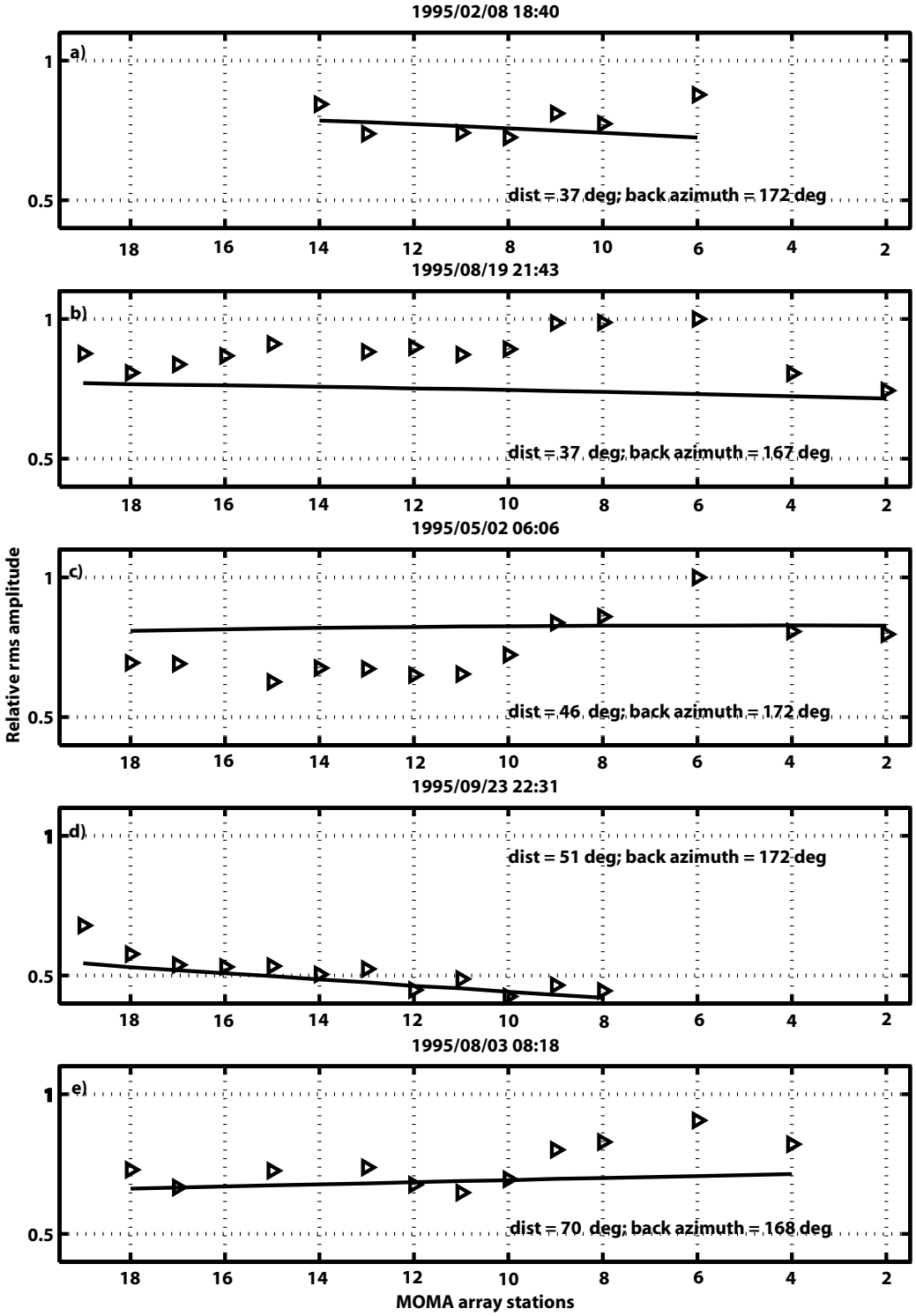


**Figure 6.** Each subplot (a to e) represents one of the five 1995 earthquakes recorded at the MOMA array and presented in Table 3. The x-axis numbers stations from 1 to 18 from East to West. The solid line represents the variation of the source radiation factor at each station. The triangles represent the rms amplitude (normalized to the largest value observed at all stations, including MOMA) for each event.

$Q_P = 600$. Variations in path length (because of different slowness) cause attenuation differences of less than 1 per cent.

We conclude that the amplitude variations are acquired by (de)focusing somewhere along the ray path. Evidence for heterogeneity is presented by Fouch *et al.* (2000) who observed differences in SKS mantle anisotropy and radial discontinuities in mantle velocity beneath the MOMA array stations. They explained the observations by proposing the existence of a keel of seismically fast

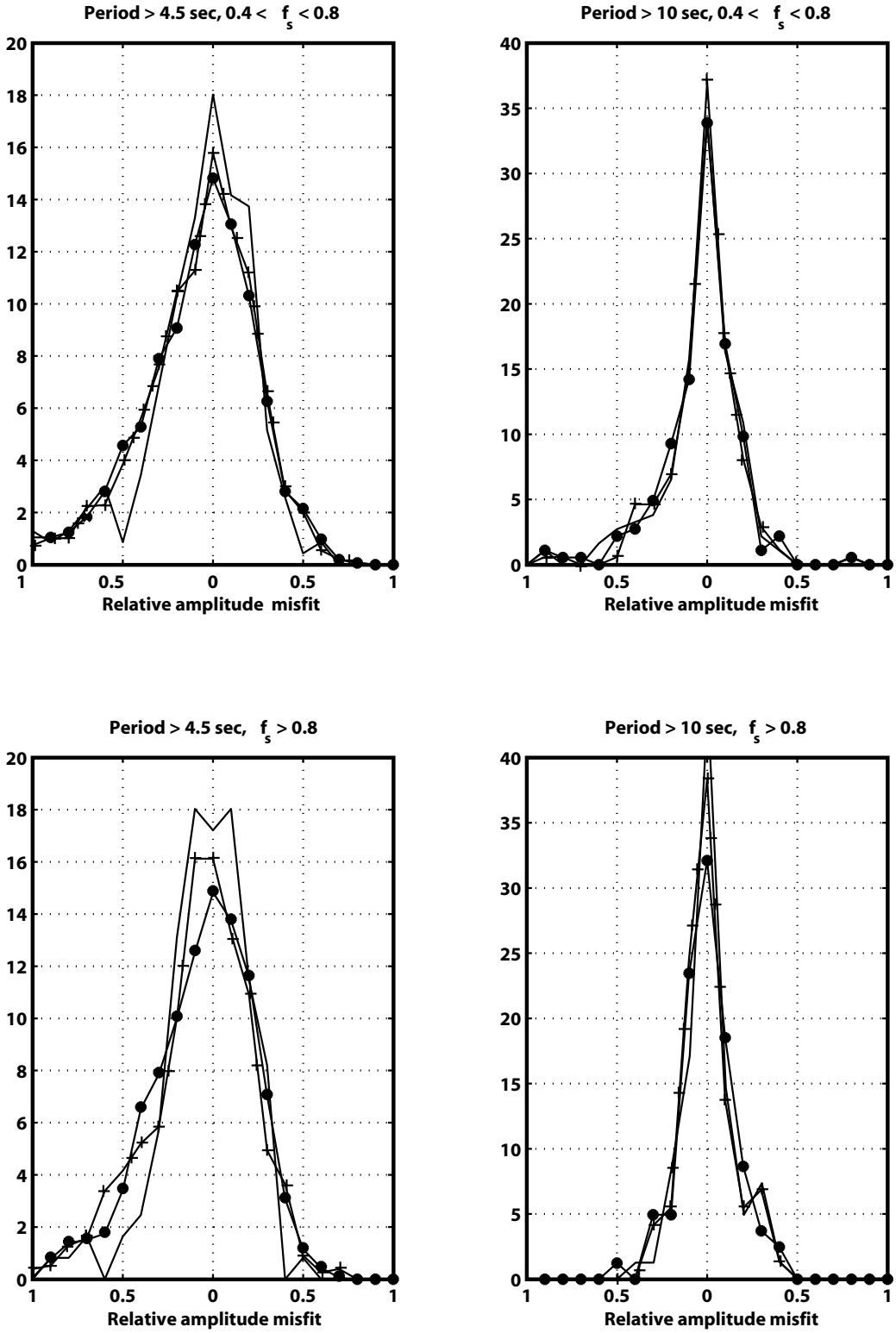


**Figure 7.** The misfit between the observed and predicted amplitude for pulse length of at least 4.5 s (left top and bottom) and more than 10 s (right top and bottom) and for source radiation factor between 0.4 and 0.8 (top subplots) and larger than 0.8 in the bottom subplots. Solid line: model IASP91, broken line: model A, dotted line: model B. The vertical axis is arbitrary but each histogram integrates to 1.

mantle that extends to depths of 300 km or more beneath the interior of the North American continent. The six easternmost MOMA stations are located at the edge and to the east of the fast continental keel structure. Our data shows a clear jump in amplitude values between the eastern and western stations. Such a deep keel is not present in the *S* wave model NA95 (Van der Lee & Nolet 1997), but if it exists it could clearly lead to focusing and defocusing at its edges, visible over a range of MOMA stations.

## 6 COMPARISON WITH GLOBAL MODELS

The difference between the predictions for models IASPEI91, A and B and the observed amplitude is presented for two cases: data with a pulse length greater than 4.5 s and those with pulses longer than 10 s. The fit between the observed and predicted energy is significantly improved when using station corrections. Generally a better fit is obtained for the subset of data with pulse length greater than 10 s, but even so there is no significant difference between IASPEI91 and the 3-D models. We also investigate the influence of errors in the source radiation factor by presenting a subset with data for which $f_s > 0.8$, minimizing the effect of errors in the source mechanism. Fig. 7 presents the relative amplitude misfit for pulse length of 4.5 s (left top and bottom) and 10 s (right top and bottom) for source radiation factor less than 0.8 (top subplots) and larger than 0.8 in the bottom subplots. The fit is not much better for cases when we make sure the radiation factor is large, confirming our earlier conclusions that errors in the moment tensors are not a major contribution to the misfits.

The sample standard deviations for the relative amplitude misfit $(A_{\rm obs} - A_{\rm pred})/A_{\rm obs}$ for the three models are presented in Table 4. Even when we take into account that Models A and B were not originally designed to predict amplitude variations, the complete lack of improvement in the predicted amplitudes for the 3-D models comes as a surprise.

## 7 CONCLUSIONS

We have analysed a database of *P* wave displacement amplitudes from the new global network of high quality digital broadband stations. Efforts have been made to reduce errors in the amplitude data introduced by source complexity, radiation pattern and source structure. For the simple waveforms for intermediate and deep earthquakes used in this study, observational errors in amplitude measurements are about 5 per cent, far less than the observed variation of 38 per cent. There is a misfit between the observed and predicted amplitude that is not significantly different whether we trace rays through a symmetrical earth model or through modified versions of existing 3-D tomographic models. We consider this as a compelling argument suggesting that there is 3-D structure in the mantle causing strong focusing and defocusing of seismic energy that is not yet modelled by the current generation of 3-D models. The fact that the variance decreases with increasing period indicates that wave front healing may play a role, i.e. that the heterogeneities responsible for the amplitude anomalies are smaller than the width of the Fresnel zone. Unfortunately, our limited data set does not allow us to make a global study of mismatches, with an analysis of where the 3-D models are most deficient. The standard deviations listed in Table 4 do however provide a yardstick to judge the adequacy of global models to represent accurate amplitudes of velocity perturbations. We note that the variations we observe are significantly larger than earlier estimates of the effects of focusing of 15 per cent by Lay & Helmberger (1981) or 25 per cent by Liu & Tromp (1996). The actual tomographic models fail to predict small variations mainly because the predicted focusing is far too small.

**Table 4.** Standard deviation (relative amplitude anomalies).

| Periods | Model A | Model B | IASPEI91 |
|---|---|---|---|
| >4.5 sec | 0.37 | 0.37 | 0.38 |
| >10 sec | 0.20 | 0.20 | 0.19 |

The limitation to deep events may bias our data towards larger amplitude anomalies than is representative for the average Earth. A separate study of shallow event amplitudes, using a different methodology to account for P-pP interference, has just been started.

Recently, Dahlen & Baig (2002) have derived Frechet kernels for body wave amplitudes. Eventually, we plan to utilize amplitudes from both shallow and deep events in a joint inversion of amplitude and delay times in a global tomographic inversion.

## ACKNOWLEDGMENTS

I. M. T and C. M. were financially supported by the NSF under contract EAR9814570. We also wish to thank the many anonymous operators of GSN as well as Karen Fisher and co-workers in the MOMA array project, and IRIS for greatly facilitating the collection of the new, superb, digital broadband data that are revolutionizing seismology.

## REFERENCES

Booth, D.C., Marshall, P.D. & Young, J.B., 1974. Long and Short Period *P*-wave amplitudes from Earthquakes in the Range 0–114 degrees, *Geophys. J. R. astr. Soc.,* 523–537.

Cerveny, V., Molotkov, I.A. & Psencik, I., 1977. *Ray Method in Seismology,* Charles University Press, Praha, p. 214.

Choy, G.L. & Cormier, V.F., 1986. Direct Measurement of the Mantle Attenuation Operator From Broadband *P* and *S* waveforms, *J. geophys. Res.,* **91,** 7326–7342.

Dahlen, F.A & Tromp, J., 1998. *Theoretical Global Seismology,* pp. 685–686, Princeton University Press, Princeton, New Jersey.

Dahlen, F.A. & Baig, A.M., 2002. Fréchet kernels for body wave amplitudes, *Geophys. J. Int.,* **150,** 440–466.

Der, Z., McElfresh, T.W. & Anne O'Donnel, 1982. An Investigation of the regional variations and frequency dependence of anelastic attenuation in the mantle under the United States in the 0.5–4 Hz band, *Geophys. J. R. astr. Soc.,* **69,** 67–99

Douglas, A., Young, J.B. & Marshall, P.D., 1981. Some analysis of P and Rayleigh wave amplitudes observed at North American stations, *Geophys. J. R. astr. Soc.,* **67,** 305–324.

Fisher, K.M. *et al.* 1996. The 1995–1996 Missouri to Massachusetts Broadband Seismometer Deployment, *IRIS Newsletter,* **15,** 6–9.

Fouch, M.J., Fisher, K.M., Parmentier, E.M., Wysession, M.E. & Clarke, T.J., 2000. Shear wave splitting, continental keels and patterns of mantle flow, *J. geophys. Res.,* **105,** 6255–6275.

Haddon, R.A. & Husebye, E.S., 1978. Joint interpretation of *P*-wave time and amplitude anomalies in terms of lithospheric heterogeneities, *Geophys. J. R. astr. Soc.,* **55,** 19–43.

Kennett, B.L.N., ed., 1991. *IASPEI 1991 Seismological Tables,* pp. 166–167, ed. Kennett, B.L.N., Research School of Earth Sciences, Australian National University, Canberra, Australia.

Lay, T. & Helmberger, D.V., 1981. Body wave amplitude patterns and upper mantle attenuation variations across North America, *Geophys. J. R. astr. Soc.,* **66,** 691–726.

Liu, F.-X. & Tromp, J., 1996. Uniformly valid body-wave ray theory, *Geophys. J. Int.,* **127,** 461–491.

Marshall, P.D., Bingham, J. & Young, J.B., 1986. An analysis of *P* wave amplitudes recorded by seismological stations in the USSR, *Geophys. J. R. astr. Soc.,* **84,** 71–91.

Masters G., Bolton, H. & Laske, G., 1999. Joint Seismic Tomography for P and S Velocities: How Pervasive are Chemical Anomalies in the Mantle?, *EOS, Trans. Am. geophys. Un.,* **80,** S14.

Nolet, G. & Dahlen, F.A., 2000. Wavefront healing and the evolution of seismic delay times, *J. geophys. Res.,* **105,** 19 043–19 054.

Pankow, K.L. & Lay, T., 2002. Modeling *S* wave amplitude patterns for events in the Kurile slab using three-dimensional Gaussian beams, *J. geophys. Res.* DOI 10.1029/2001JB000594 2194.

Romney, C., 1959. Amplitudes of Seismic Body Waves from Underground Nuclear Explosions, *J. geophys. Res.,* **64,** 1489–1498.

Van der Hilst, R.D., Widiyantoro, S. & Engdahl E.R., 1997. Evidence for deep mantle circulation from global tomography, *Nature,* **386,** 570–584.

Van der Lee, S. & Nolet, G., 1997. Upper mantle S velocity structure of North America, *J. geophys. Res.,* **102,** 22 815–22 838.

Zhou, Y., Nolet, G. & Dahlen, F.A., 2002. Surface sediment effects on teleseismic *P* wave amplitude, *J. geophys. Res.,* in press.